Data assimilation in a baroclinic coastal ocean model: ensemble statistics and comparison of methods

A. L. Kurapov, G. D. Egbert, R. N. Miller, and J. S. Allen

College of Oceanic and Atmospheric Sciences,

Oregon State University,

104, Ocean Adm. Bldg, Corvallis, OR, 97331-5503

kurapov@oce.orst.edu

March 20, 2002

Published in *Monthly Weather Review*, Vol. 130, No. 4, 1009-1025.

Abstract

The performance of data assimilation methods in an idealized three-dimensional time-dependent coastal baroclinic model is assessed by computing ensemble error statistics. The analytical representer solution allows us to compute posterior error statistics for the variational generalized inverse method (GIM) as well as sequential methods such as the Kalman filter (KF) and optimal interpolation (OI). Computations can be made in a straightforward way, given the statistics of errors in the model equations and data. The GIM yields solutions with significantly smaller variance than that given by KF or OI if the data contain valuable information about the past flow. This is the case, for instance, when a large fraction of model error is due to uncertainty in the wind stress. In the scope of our model, we analyze the plausibility of simplifications made in a practical OI scheme. The unified study of the GIM, KF, and OI allowed us to demonstrate how the forecast error covariance used in a practical OI sequential scheme may be optimized with the use of lagged covariances for the model solution. We also assess the effect of the misspecified input error statistics on the solution quality. In some practically relevant cases the use of future data by the GIM, in contrast to KF and OI, compensates for incorrectly specified input error covariances.

1 Introduction

Data assimilation can be an expensive business in terms of both computational time and storage (Talagrand 1997). Given the present state of the art, coastal dynamical models are complicated to such a degree that simplified data assimilation techniques are generally required to make computations feasible. We find it is important to understand how different simplifications affect the quality of the solution in the context of coastal ocean data assimilation.

The problem of finding the best estimate of an entire time series, given a prior estimate and a series of observations of that time series, is known as the smoothing problem (Bennett 1992, p. 112). The generalized inverse method (GIM), a variational data assimilation

scheme, can be used to find a solution to a smoothing problem that is optimal in a least square sense. The GIM yields a solution minimizing a cost functional that is a sum of penalties on errors in the inputs such as the model, initial and boundary conditions, and the data. From a Bayesian statistical perspective the method seeks the most probable state in the space of possible solutions. In the linear Gaussian case this is equivalent to minimizing the error variance of the solution at each point, and at each time. Estimates of the error covariances of the inputs are required for the definition of the penalty terms, and are prerequisites for obtaining the optimal solution. The GIM uses the model as a dynamically based interpolator between the data, providing correction to the model solution globally in space and time. If the measurements contain valuable information about the flows in the past or the future, perhaps somewhere distant from the measurement locations, this information will be acknowledged and "transmitted" by the model. In this way estimates of initial and open boundary values may be improved substantially.

Another class of data assimilation methods are solutions to the "filtering problem", *i.e.*, the problem of finding the best estimate of a time series at a given time, which we may call the "present", given only previous and contemporaneous observations, but no subsequent or "future" observations (see Bennett 1992, p. 90). The Kalman filter (KF) gives the solution to the optimal filtering problem (Gelfand and Fomin 1963; Miller 1996). It is a sequential algorithm: the model is run forward, and when the measurements are available, the forecast is corrected by extrapolating forecast-data discrepancies to all state variables. Thus, data assimilation is done in repeated cycles: forecast (model run) followed by correction (analysis). Extrapolation from the data to the full state space is accomplished by means of a gain matrix which evolves with time in such a way that the analysis field has minimum error variance conditional on all past data. Note that at each stage only present data are used for the correction. So, the KF does not require retention of past data. All of the influence of past data is embedded in the evolution of the forecast error covariance. The KF, like the GIM, requires specification of the input error covariances. In the linear case, the KF yields the same result as the GIM after the

last data in a series of measurements are assimilated, but remains in general sub-optimal compared to the GIM at earlier steps. Filtering methods are especially useful in such applications as numerical weather prediction, in which going back and correcting past estimates is of limited interest.

In oceanographic research, the task is often to reconstruct past flows with the goal of understanding underlying dynamical processes, rather than producing forecasts. In this case, to recover the true flow at any particular time, it would be sensible to use all available data. However, computational costs limit use of GIM with realistic models. In particular, a literal application of the theory would require storage of the model error term at every spatial node and at every time step of the integration period. Computational costs are also a big obstacle for use of KF. Although the scheme is sequential and does not require storing model errors for all times, the equations for the forecast error covariance matrix, of size $M \times M$, where M is the length of the state vector, must be integrated in time. Exact implementation of such a scheme for a realistic oceanographic model would obviously be impractical.

As an approximation to the KF, optimal interpolation (OI; *cf.* Daley 1991, p. 98), has been developed. For example, Oke et al. (2001) used an OI scheme to assimilate HF radar surface current data into a primitive equation model of circulation on the mid-Oregon shelf. The gain matrix was not evolved from one assimilation cycle to the next, so the cost of computation was not significantly higher than for a simple forward model run. However, for OI, the gain matrix still must be chosen somehow. From a statistical perspective, the optimal stationary gain matrix would be the limiting (as $t \to \infty$) KF forecast error covariance, which typically becomes stationary after a long period of integration. Instead of deriving this stationary forecast error covariance (a challenging task for a primitive equation model), Oke et al. (2001) used a scaled model solution error covariance. This was computed from averaging over an ensemble of model simulations for 18 different summers forced with observed winds. Thus, it was assumed that data assimilation reduced the error variance of the forecast in comparison with that of the prior model, but left the correlation

structure of the errors unchanged. Although *ad hoc*, this scheme has the virtue of yielding an anisotropic inhomogeneous forecast error covariance with dynamically sensible length scales consistent with local topography.

In oceanography, the amount of empirical information is never sufficient to specify the statistics of the model errors completely. Accuracy of the data is sometimes also difficult to assess, particularly as we must allow for the limited ability of our models to represent the actual data. For example, our ability to represent surface currents from the HF radars will depend critically on the accuracy of our model representation of the surface mixed layer. So, the choice of the input error statistics is always a hypothesis. Possible misspecifications of these statistics will affect the performance of any DA system.

Here we analyze GIM, KF, and OI in a unified framework to gain insights into several important questions in coastal data assimilation. We address the following issues: how useful future data are for prediction of the flow at a particular time; what the optimal gain matrix for OI should be, and how sensitive the performance of OI is to this choice; and how misspecified input error covariances affect the quality of the solutions. A thorough answer to these questions would be difficult to obtain in the context of a model based on the full primitive equations, so our analysis will be based on the idealized coastal dynamical model described in the companion paper (Kurapov et al. 2001, manuscript submitted to *J. Geophys. Res. – Oceans*, hereafter KAME). As application of this simplified model to real data would probably not be instructive, we pursue a theoretical analysis. In KAME we performed experiments with synthetic data to illuminate some fundamental issues in coastal data assimilation such as restoration of the open boundary conditions and sensitivity of the solution to the choice of weights in the cost functional. The quality of the solution in such experiments depends on the choice of the "true" wind forcing and on initial and boundary conditions. Here, a more general approach, based on the methodology of estimation theory (Cohn 1997), is used. We compute the error statistics of ensembles of solutions to compare the performance of data assimilation methods. For our simple linear model, results may be computed exactly in a straightforward way given

the error statistics of the inputs. The advantage of this approach is that the ensemble of actual solutions does not have to be generated, so results are independent of the choice of mean and sampling strategy. The representer functions, obtained analytically in KAME as components of the generalized inverse solution, yield the error covariance of the model solution, given input error statistics. Using these analytic expressions, posterior error analysis requires only simple matrix manipulations. The computations for the GIM- and KF-derived solutions are standard (see Bennett 1992, §5.6). We will need to devise some new tools to compute the posterior error statistics for OI, and to assess the effect of incorrect input error statistics for all the methods.

In Section 2, we give a comparative description of GIM, KF, and OI with the emphasis on how the solution error covariance can be computed. In Section 3, we describe briefly the coastal inverse model. In Section 4, results of variance computations are presented, including a discussion of possible choices for the gain matrix in OI. The effect of incorrect input error statistics on the performance of the inverse solution is considered in Section 5. Finally, Section 6 contains a summary and discussion.

2 Posterior statistics

The goals of this section are to establish the optimal form of the gain matrix for OI, relate this to GIM and KF, and compute the error statistics of the OI-derived solution. We derive these results for a general model of the form commonly used in theoretical studies on data assimilation (see, *e.g.*, Miller 1996; Cohn 1997):

$$\mathbf{u}_{t+1} = \mathbf{A}\mathbf{u}_t + \boldsymbol{\epsilon}_{t+1}, \tag{1}$$

where $\mathbf{u}_t$ is the true solution at time t, $\mathbf{A}$ is a model operator that propagates the solution forward from time t to time $t+1$, and $\boldsymbol{\epsilon}_{t+1}$ denotes model error. $\mathbf{A}$ includes necessary boundary conditions. Measurements are taken regularly at the same N locations at times $t = 1, 2, \ldots, T$:

$$\mathbf{d}_t = \mathbf{H}\mathbf{u}_t + \boldsymbol{\eta}_t, \tag{2}$$

where $\mathbf{H}$ is the data operator, and vectors $\mathbf{d}_t$ and $\boldsymbol{\eta}_t$ (of length N) represent data values and errors, correspondingly. In the present study, both $\mathbf{A}$ and $\mathbf{H}$ are linear and time-independent.

To simplify the presentation, we will consider the model (1) to be discretized on a computational grid such that $\mathbf{u}_t$ and $\boldsymbol{\epsilon}_t$ are vectors of length M while $\mathbf{A}$ and $\mathbf{H}$ are matrices of size $M \times M$ and $N \times M$, respectively. The same analysis holds for continuous $\mathbf{u}$, provided the matrix transpose $\mathbf{A}'$ is interpreted as the adjoint.

The model and data errors are assumed to be unbiased random variables with covariances

$$\overline{\boldsymbol{\epsilon}_s \boldsymbol{\epsilon}_t'} = \begin{cases} \boldsymbol{\Pi}_t, & \text{if } s = t, \\ 0 & \text{if } s \neq t, \end{cases} \tag{3}$$

$$\overline{\boldsymbol{\eta}_s \boldsymbol{\eta}_t'} = \begin{cases} \sigma^2 \mathbf{I}_N & \text{if } s = t, \\ 0 & \text{if } s \neq t. \end{cases} \tag{4}$$

Here, the overbar denotes ensemble averaging. The errors are assumed to be uncorrelated in time, although a more general treatment for the GIM and KF would be possible. In (4), the data are all assumed to have constant error variance σ^2; $\mathbf{I}_N$ is the diagonal identity matrix of size $N \times N$. A more general, non-diagonal and time dependent data error covariance would not alter the derivation, but would make notation more cumbersome.

Since the error covariance of the inverse solution, or *posterior covariance*, would not depend on the forcing and prior guesses for initial/boundary conditions, a homogeneous problem is considered. In particular, $\mathbf{u}_0 = 0$, and the prior model solution $\mathbf{u}^{model} = 0$. The initial condition is satisfied exactly. The error covariance of the model solution, or *prior covariance*, is:

$$\mathbf{P}_{s,t} \equiv \overline{(\mathbf{u}_s - \mathbf{u}_s^{model})(\mathbf{u}_t - \mathbf{u}_t^{model})'} = \overline{\mathbf{u}_s \mathbf{u}_t'} = \sum_{i=1}^{\min(s,t)} \mathbf{A}^{s-i} \boldsymbol{\Pi}_i (\mathbf{A}^{t-i})'. \tag{5}$$

For $m \geq n$, (5) yields

$$\mathbf{A}\mathbf{P}_{m,n} = \mathbf{P}_{m+1,n}, \tag{6}$$

i.e. the prior covariance is propagated forward in time by the model operator.

Note, that throughout this presentation the term "prior covariance" is used for the covariance of the error in the prior model *solution*, rather than the covariance of errors in the prior model *equations* ($\mathbf{\Pi}_i$). Before proceeding with our treatment of OI, it is instructive and useful to review GIM and KF. Our analytical solution for the representers needed for GIM (KAME) provides expressions for all elements of $\mathbf{P}_{s,t}$, which in turn can be used in computation of the posterior error statistics for KF and OI. Also, by considering the KF, we will see how to construct the optimal gain matrix for OI.

2.1 Generalized inverse

For our generic model (1) the cost function to minimize is

$$J(\mathbf{u}_1, \mathbf{u}_2, ..., \mathbf{u}_T) = \sum_{t=1}^{T} (\boldsymbol{\epsilon}_t' \mathbf{\Pi}_t^{-1} \boldsymbol{\epsilon}_t + \sigma^{-2} \boldsymbol{\eta}_t' \boldsymbol{\eta}_t). \tag{7}$$

where $\boldsymbol{\epsilon}_t$ and $\boldsymbol{\eta}_t$ are the estimates of the model and data errors. The inverse solution can be written in terms of the data and representers as

$$\tilde{\mathbf{U}} = \mathbf{Q}(\mathbf{R}_T + \sigma^2 \mathbf{I}_{NT})^{-1} \mathbf{D}_T, \tag{8}$$

where

$$\tilde{\mathbf{U}} = \begin{pmatrix} \tilde{\mathbf{u}}_1 \\ \tilde{\mathbf{u}}_2 \\ \vdots \\ \tilde{\mathbf{u}}_T \end{pmatrix}, \tag{9}$$

$$\mathbf{D}_T = \begin{pmatrix} \mathbf{d}_1 \\ \mathbf{d}_2 \\ \vdots \\ \mathbf{d}_T \end{pmatrix}, \tag{10}$$

$$\mathbf{Q} = \begin{pmatrix} \mathbf{Q}_{1,1} & \mathbf{Q}_{1,2} & \cdots & \mathbf{Q}_{1,T} \\ \mathbf{Q}_{2,1} & \mathbf{Q}_{2,2} & \cdots & \mathbf{Q}_{2,T} \\ \vdots & \vdots & \ddots & \vdots \\ \mathbf{Q}_{T,1} & \mathbf{Q}_{T,2} & \cdots & \mathbf{Q}_{T,T} \end{pmatrix}, \tag{11}$$

and the blocks $\mathbf{Q}_{m,n} = \mathbf{P}_{m,n}\mathbf{H}'$ are each matrices, of size $M \times N$, so $\mathbf{Q}$ is of size $MT \times NT$. Each column of (11) is the representer corresponding to a particular datum; together $\mathbf{Q}_{1,t}, \ldots, \mathbf{Q}_{T,t}$ give N representers for all the data measured at time t. For point measurements $\mathbf{P}_{m,n}\mathbf{H}'$ is just selected columns of $\mathbf{P}_{m,n}$.

The representer matrix $\mathbf{R}_T$ is of size $NT \times NT$, composed of blocks $\mathbf{R}_{m,n} = \mathbf{H}\mathbf{P}_{m,n}\mathbf{H}'$. In the following, we will use special notation for a row of blocks of $\mathbf{Q}$ to the left of the diagonal blocks $\mathbf{Q}_{t,t}$:

$$\mathbf{S}_t = (\mathbf{Q}_{t,1}|\mathbf{Q}_{t,2}|\ldots|\mathbf{Q}_{t,t-1}). \tag{12}$$

This matrix represents lagged error covariances of the model solution at time t with the solution at all earlier measurement times. For lagged covariances, (6) yields

$$\mathbf{A}(\mathbf{S}_t|\mathbf{Q}_{t,t}) = \mathbf{S}_{t+1}. \tag{13}$$

The posterior covariance for all state variables, at all times, is

$$\overline{(\mathbf{U} - \tilde{\mathbf{U}})(\mathbf{U} - \tilde{\mathbf{U}})'} = \overline{\mathbf{U}\mathbf{U}'} - \mathbf{Q}(\mathbf{R}_T + \sigma^2\mathbf{I}_{NT})^{-1}\mathbf{Q}', \tag{14}$$

where the first term on the r.h.s. is the prior covariance, a block matrix analogous to $\mathbf{Q}$ but with entries $\mathbf{P}_{m,n}$. In particular, at time $t = T$, the inverse solution is

$$\tilde{\mathbf{u}}_T = (\mathbf{S}_T|\mathbf{Q}_{T,T})(\mathbf{R}_T + \sigma^2\mathbf{I}_{NT})^{-1}\mathbf{D}_T, \tag{15}$$

and the posterior covariance for all state variables, at time T, is

$$\mathbf{P}^{GIM}_{T,T} = \overline{(\mathbf{u}_T - \tilde{\mathbf{u}}_T)(\mathbf{u}_T - \tilde{\mathbf{u}}_T)'} = \mathbf{P}_{T,T} - (\mathbf{S}_T|\mathbf{Q}_{T,T})(\mathbf{R}_T + \sigma^2\mathbf{I}_{NT})^{-1}(\mathbf{S}_T|\mathbf{Q}_{T,T})'. \tag{16}$$

2.2 Kalman Filter

The KF solution, or analysis, at time t, is usually expressed as (see Miller 1996):

$$\mathbf{u}^a_t = \mathbf{A}\mathbf{u}^a{}_{t-1} + \mathbf{G}_t(\mathbf{d}_t - \mathbf{H}\mathbf{A}\mathbf{u}^a_{t-1}). \tag{17}$$

The gain matrix $\mathbf{G}_t$ is

$$\mathbf{G}_t = \mathbf{C}_t\mathbf{H}'(\mathbf{H}\mathbf{C}_t\mathbf{H}' + \sigma^2\mathbf{I}_N)^{-1}, \tag{18}$$

where $\mathbf{C}_t$ is the forecast error covariance:

$$\mathbf{C}_t = \overline{(\mathbf{u}_t - \mathbf{A}\mathbf{u}^a_{t-1})(\mathbf{u}_t - \mathbf{A}\mathbf{u}^a_{t-1})'} = \mathbf{A}\mathbf{P}^a_{t-1}\mathbf{A}' + \mathbf{\Pi}_t. \tag{19}$$

From a statistical viewpoint, $\mathbf{C}_t$ is the covariance of the model solution conditioned upon the past data.

An analysis error covariance, or posterior covariance, is:

$$\mathbf{P}^a_t = \mathbf{C}_t - \mathbf{G}_t\mathbf{H}\mathbf{C}_t. \tag{20}$$

To run the KF from $t-1$ to t, the analysis field $\mathbf{u}_{t-1}$ and the analysis error covariance $\mathbf{P}^a_{t-1}$ are necessary. One can show that at time T, when the last measurements are available, $\mathbf{u}^a_T = \tilde{\mathbf{u}}_T$, and $\mathbf{P}^a_T = \mathbf{P}^{GIM}_{T,T}$. This is intuitively obvious, since the KF makes optimal use of all prior data, and the GIM of all data.

In practice, updating the forecast covariance (19) is the most demanding computation. However, if the matrix $\mathbf{Q}$ is known, as for instance when the representer solution is

available, there is no need in applying (19) each assimilation cycle. If the goal is to reproduce the result of the KF given the representer solution, $\mathbf{C}_t$ can be computed as

$$\mathbf{C}_t = \mathbf{P}_{t,t} - \mathbf{S}_t(\mathbf{R}_{t-1} + \sigma^2 \mathbf{I}_{N(t-1)})^{-1}\mathbf{S}_t'. \tag{21}$$

To prove (21), use (19) and first note that $\mathbf{P}^a_{t-1}$ is equal to the r.h.s. of (16), where T is replaced by $t-1$; then, apply (5) and (13). All the entries in (21) are given by the representer solution. $\mathbf{R}_{t-1}$, of size $N(t-1) \times N(t-1)$, is the upper left corner of the representer matrix. Note that while both $\mathbf{C}_t$ and $\mathbf{P}_{t,t}$ are matrices of large dimension $(M \times M)$, to find the solution we need to operate only with $\mathbf{C}_t\mathbf{H}'$ and $\mathbf{P}_{t,t}\mathbf{H}'$, which are much smaller since generally $N \ll M$.

2.3 Optimal Interpolation (OI)

By OI we mean a simplified sequential data assimilation method such that the gain matrix is not changed from one assimilation cycle to the next. As time goes on, the dimension of $\mathbf{S}_t$ in (21) increases. $\mathbf{C}_t$ will become stationary for large t if $\mathbf{P}_{t,t}$ does, and if the lagged covariances $\mathbf{Q}_{n,t}$ are negligible for large $t-n$. In this case $\mathbf{G}_t \to \mathbf{G}_\infty$, a constant gain matrix. In our numerical examples we perform data assimilation over a finite period of time. We check that $\mathbf{C}_t$ stabilizes by the end of the assimilation period (T), and take the limiting gain matrix $\mathbf{G}_T \equiv \mathbf{G}$ as optimal for OI.

Oke et al. (2001) essentially approximated $\mathbf{C}_T\mathbf{H}'$ by $a\mathbf{P}_{T,T}\mathbf{H}'$, where $a = \text{const} < 1$. The estimate of $\mathbf{P}_{T,T}\mathbf{H}'$ was obtained utilizing time averaged correlations of model solutions computed with observed winds for 18 different summers. Thus, the assumption was made that the correlation structure of the prior error covariance conditioned upon the past data, $\mathbf{C}_T$, was the same as that of the unconditional prior error covariance, $\mathbf{P}_{T,T}$. To explore the possible consequences of this assumption, we need to compute the posterior covariance of OI solution for gain matrices based on $\mathbf{C}_T$ and $a\mathbf{P}_{T,T}$. We refer to results for these two as cases "OI(C)" and "OI(aP)", respectively.

From (15), the OI solution can be written as

$$\mathbf{u}_t^a = \mathbf{K}\mathbf{D}_t, \tag{22}$$

where $\mathbf{D}_t$ is the vector of all data available to time t (see (10));

$$\mathbf{K} = (\mathbf{C}^{t-1}\mathbf{G}|\mathbf{C}^{t-2}\mathbf{G}|\ldots|\mathbf{G}) \tag{23}$$

is a matrix of size $M \times Nt$, and

$$\mathbf{C} = \mathbf{A} - \mathbf{G}\mathbf{H}\mathbf{A}. \tag{24}$$

The posterior covariance is then

$$\overline{(\mathbf{u}_t - \mathbf{u}_t^a)(\mathbf{u}_t - \mathbf{u}_t^a)'} = \overline{\mathbf{u}_t\mathbf{u}_t'} - \overline{\mathbf{u}_t\mathbf{u}_t^{a\prime}} - \overline{\mathbf{u}_t^a\mathbf{u}_t'} + \overline{\mathbf{u}_t^a\mathbf{u}_t^{a\prime}} \quad =$$

$$= \mathbf{P}_{t,t} - (\mathbf{S}_t|\mathbf{Q}_{t,t})\mathbf{K}' - \mathbf{K}(\mathbf{S}_t|\mathbf{Q}_{t,t})' + \mathbf{K}(\mathbf{R}_t + \sigma^2\mathbf{I}_{Nt})^{-1}\mathbf{K}'. \tag{25}$$

To make use of (25), we need an explicit form for $\mathbf{K}$, and we thus must compute $\mathbf{C}^s\mathbf{G}$. Further derivation depends on the choice of $\mathbf{G}$. In the case of OI(aP), $\mathbf{G} = \mathbf{P}_{T,T}\mathbf{H}'\mathbf{\Omega}$, where

$$\mathbf{\Omega} = (\mathbf{R}_{T,T} + a^{-1}\sigma^2\mathbf{I}_N)^{-1}. \tag{26}$$

Properties (6) and (13) are used to obtain

$$\mathbf{C}^s\mathbf{G} = \sum_{i=0}^{s} \mathbf{Q}_{T+i,T}\mathbf{B}_{s-i}, \tag{27}$$

where

$$\mathbf{B}_n = \begin{cases} \mathbf{\Omega} & \text{if } n = 0, \\ -\mathbf{\Omega}\sum_{i=1}^{n} \mathbf{R}_{T+i,T}\mathbf{B}_{s-i} & \text{if } n > 0, \end{cases} \tag{28}$$

which is computed recursively.

In the case of OI(C), $\mathbf{G} = \mathbf{C}_T\mathbf{H}'\hat{\mathbf{\Omega}}$, where $\hat{\mathbf{\Omega}} = (\mathbf{H}\mathbf{C}_T\mathbf{H}' + \sigma^2\mathbf{I}_N)^{-1}$. In (27) and (28), we use $\hat{\mathbf{\Omega}}$, $\hat{\mathbf{Q}}_{T+i,T}$, and $\hat{\mathbf{R}}_{T+i,T}$ instead of $\mathbf{\Omega}$, $\mathbf{Q}_{T+i,T}$, and $\mathbf{R}_{T+i,T}$, where

$$\hat{\mathbf{Q}}_{T+i,T} = \mathbf{Q}_{T+i,T} - \sum_{n=1}^{T-1} \mathbf{Q}_{T+i,n}\mathbf{Z}'_n, \tag{29}$$

$$\hat{\mathbf{R}}_{T+i,T} = \mathbf{R}_{T+i,T} - \sum_{n=1}^{T-1} \mathbf{R}_{T+i,n}\mathbf{Z}'_n, \tag{30}$$

and $\mathbf{Z}_n$ are blocks of size $N \times N$ that form the matrix $(\mathbf{Z}_1|\mathbf{Z}_2|\ldots|\mathbf{Z}_{T-1}) = \mathbf{H}\mathbf{S}_T(\mathbf{R}_{T-1} + \sigma^2\mathbf{I}_{N(T-1)})^{-1}$. Using the analytical representer solution and (26)-(30) we can explicitly construct $\mathbf{K}$ (23) and hence posterior covariances (25) for both the OI(C) and OI(aP) cases.

3 Inverse coastal model

Here we give a summary of the coastal model described in detail in KAME. A number of simplifications are made to make analytical progress possible. We consider subinertial linear motions near a straight coast in a basin of constant depth H, with linear ambient stratification. A long-wave boundary layer approximation is made. Effects of the surface and bottom Ekman layers are parameterized. Friction is parameterized in Rayleigh form. The problem is considered in terms of the perturbation pressure p, and only the baroclinic part is retained.

All variables are made non-dimensional: time by the inverse of the Coriolis parameter f^{-1}, horizontal distance by the Rossby radius of deformation NH/f, where N is the buoyancy frequency. Our computational domain represents a part of the North American western coast, with the x-axis of the coordinate system directed offshore ($0 \leq x < \infty$), the y-axis toward the south along the coast($0 \leq y \leq L$), and the z-axis vertical ($0 \leq z \leq 1$) (Fig. 1).

The model equation and associated boundary/initial conditions are:

$$\left(\frac{\partial}{\partial t}+\alpha_m\right)(p_{xx}+p_{zz}) = \quad \epsilon^{(m)}, \tag{31}$$

$$p_{xt}+p_y+\alpha_c p_x = (\delta(z-1)-1)\hat{\tau}(y,t) \quad +\epsilon^{(c)} \quad \text{at } x=0, \tag{32}$$

$$p_{zt}=0 \quad \text{at } z=0 \text{ or } z=1, \tag{33}$$

$$p_{xx}+p_{zz}=Q(x,y,z) \quad +\epsilon^{(IPV)} \quad \text{at } t=0, \tag{34}$$

$$p=I(y,z) \quad +\epsilon^{(I)} \quad \text{at } x=0,\ t=0, \tag{35}$$

$$p=B(z,t) \quad +\epsilon^{(B)} \quad \text{at } x=0,\ y=L, \tag{36}$$

$$p\to 0 \quad \text{as } x\to\infty, \tag{37}$$

where subscripts x, y, z, and t denote partial differentiation; $\epsilon^{(\cdot)}$ on the right hand sides represent errors in the governing equation, initial and boundary conditions; $\hat{\tau}$ is the wind stress that forces surface Ekman flow next to the coast; α_m and α_c are dissipation parameters. Condition (34) is for the initial potential vorticity (IPV). Expressions (35) and (36) provide initial and boundary conditions for coastal trapped baroclinic waves that travel from the south ($y=L$) to the north ($y=0$). In the analysis of the second-order posterior statistics below we assume homogeneous initial and boundary conditions, and no forcing in (32). Error-free boundary conditions at the surface and bottom (33) are assumed so that p and $\epsilon^{(\cdot)}$ can be obtained as a series of cosine baroclinic modes. For instance,

$$p=\sum_{n=1}^{\infty}(-1)^n p_n(x,y,t)\cos(n\pi z). \tag{38}$$

We assume direct measurements of the pressure $p(x_k,y_k,z_k,t_k)=d_k$ are available, where $k=1,\ldots,K$. The cost functional is:

$$
\begin{aligned}
J(p) &= w_m \int_0^\infty dx \int_0^L dy \int_0^L dy_1 \int_0^1 dz \int_0^T dt \\
&\qquad e^{\gamma x} \epsilon^{(m)}(x,y,z,t)\, C_m^{-1}(y-y_1)\, \epsilon^{(m)}(x,y_1,z,t) + \\
&+ w_c \int_0^L dy \int_0^L dy_1 \int_0^1 dz \int_0^T dt\, \epsilon^{(c)}(y,z,t)\, C_c^{-1}(y-y_1)\, \epsilon^{(c)}(y_1,z,t) + \\
&+ w_{IPV} \int_0^\infty dx \int_0^L dy \int_0^L dy_1 \int_0^1 dz\, e^{\gamma x} \epsilon^{(IPV)}(x,y,z)\, C_{IPV}^{-1}(y-y_1)\, \epsilon^{(IPV)}(x,y_1,z) + \\
&+ w_{IB} \sum_{n=1}^{\infty} w_n \int_0^{L_n} ds \int_0^{L_n} ds_1\, p_n(y(s),t(s))\, C_n^{-1}(s-s_1)\, p_n(y(s_1),t(s_1)) + \\
&+ w_d \sum_{k=1}^{K} (p(x_k,y_k,z_k,t_k) - d_k)^2. \qquad (39)
\end{aligned}
$$

In (39) we assume the errors $\epsilon^{(m)}$, $\epsilon^{(c)}$, $\epsilon^{(IPV)}$, and $\epsilon^{(I)}$ are correlated in the alongshore direction with Gaussian covariances $C(y-y_1) = \exp(-(y-y_1)^2/L_y^2)$, where L_y is the error decorrelation length scale. Errors in the south boundary condition, $\epsilon^{(B)}$, are correlated in time. As described by the term "IB" of (39), the errors in (35) are correlated with the errors in (36) mode-by-mode, in a manner consistent with the dynamics of the long alongshore waves. In this term, integration is performed over the parametric variable s such that y first varies from 0 to L while $t = 0$, and then $y = L$ while t varies from 0 to T; $L_n = L + (n\pi)^{-1}T$. Higher weights are assigned to higher modes of $\epsilon^{(I)}$ and $\epsilon^{(B)}$ at the rate $w_n = (n\pi)^\beta$ to inhibit singular behavior of the solution at the surface. This is equivalent to assigning a specific covariance in the vertical:

$$
C(z;z_1) = \sum_{n=1}^{\infty} (n\pi)^{-\beta} \cos(n\pi z) \cos(m\pi z_1). \qquad (40)
$$

In computations, we always have $\beta = 2$ in the term "IB". In Sect. 4, we will consider a similar covariance in the vertical for $\epsilon^{(m)}$ and $\epsilon^{(IPV)}$, with $\beta = 0$ or $\beta = 2$. Terms "m" and "IB" in (39) are written for $\beta = 0$ which corresponds to assumption that the errors are not correlated in the vertical. Terms "m" and "IPV" of (39) contain exponential factors to eliminate the prior variance far offshore, as discussed in KAME.

The representers (see (8)) are computed as a sum of the baroclinic modes, and for each baroclinic mode, an analytical expression was obtained in KAME. Each representer has stationary and propagating components, the latter moving as long coastal trapped baroclinic waves.

The representer for the direct measurement of the state variable, the pressure, is exactly the prior covariance at the measurement point with all the other points in space and time (Bennett 1992; see also Appendix C in KAME). Although our analytical coastal model, continuous in space and time, does not fit immediately the discrete time used in the previous Section, these results still apply since equivalence of the continuous and discrete inverse problems can be easily established. For instance, let us consider a continuous time model of the general form

$$\frac{\partial \mathcal{B}\mathbf{u}}{\partial t} = \mathcal{A}\mathbf{u} + \mathbf{e}(t), \tag{41}$$

where $\mathcal{B}$, $\mathcal{A}$ are operators (matrices) acting on state vector $\mathbf{u}(t)$, which is here continuous in time and still discrete in space, and $\mathbf{e}(t)$ is the error in the continuous equations which is assumed to be temporally uncorrelated, with spatial covariance $\mathbf{\Psi}_t = \overline{\mathbf{e}(t)\mathbf{e}(t)'}$. Equation (41) again includes appropriate boundary conditions. Then, if the operator $\mathbf{A}^\tau$ is defined as

$$\mathbf{A}^\tau \mathbf{v} = \mathbf{u}(\tau), \tag{42}$$

where $\mathbf{u}(t)$ is the solution to

$$\frac{\partial \mathcal{B}\mathbf{u}}{\partial t} = \mathcal{A}\mathbf{u}, \tag{43}$$

$$\mathbf{u}(0) = \mathbf{v}, \tag{44}$$

and if the input error covariances for the discrete and continuous problems are related as

$$\mathbf{\Pi}_t = \int_{t-1}^{t} \mathbf{A}^{t-\nu} \mathbf{\Psi}_\nu (\mathbf{A}^{t-\nu})' \, d\nu, \tag{45}$$

then the prior error covariance computed for the discrete problem $\mathbf{P}_{s,t}$ will coincide with that for the continuous problem $\overline{\mathbf{u}(t)\mathbf{u}(s)'}$. So, there is no approximation needed to apply the discrete time matrix results to the continuous time model. Similar provisions can be made for a model continuous in space.

4 Posterior variance computations

Our coastal inverse model includes a number of parameters that will be chosen with relevance to the mid-Oregon coast where an HF radar system has been operating for the past several years (Kosro et al. 1997). In this area, a non-dimensional time interval 8 would correspond to approximately 1 day. In computations, $\alpha_m = \alpha_c = 1/24$ except for one special case discussed in Sect. 4.1. The unit non-dimensional horizontal distance will correspond to about 25 km. The HF radar system covers a region approximately 50×50 km^2, and observations are available on an hourly basis. Our zone of interest would thus be of nondimensional length $L = 2$ alongshore. We will assimilate synthetic pressure data measured from time 0 to $T = 80$ ($\sim$ 10 days) every $\delta t = 2$ at 21 points on the surface ($x_k = 0.1$, 0.3, 0.5, y_k from 0.1 to 1.9 spaced 0.3, see Fig. 1). The posterior covariance does not depend on the actual data values, but only on the data error statistics (σ^2) as well as model error statistics. In the computations, the error decorrelation length scale L_y is the same for the model, initial and boundary conditions. The performance of the methods will be assessed by comparison of the prior and posterior error variances, E_{prior} and E_{post}, as functions of spatial coordinates and time.

4.1 Performance of GIM in the vertical and time

The first question asked with regard to sea surface data assimilation is how much information such data contain about the ocean state at depth. In KAME, we tried to answer this question by performing twin experiments, with the governing equation (31) assumed to be a strong constraint. Here, we consider a weak constraint case ($w_m < \infty$) and compare

the prior and posterior variances as functions of the vertical coordinate at a particular location ($x = 0.2$, $y = 1$). Two specific questions are addressed. The first is the effect of the model error (input) covariance in the vertical (see(40)) on the performance of the inverse model at depth. The second question is the restriction of the growing error in the prior model solution with time, both at the surface and the bottom. In KAME it was shown that without dissipation in the governing equation ($\alpha_m = 0$ in (31)) the prior variance grows linearly with time. We are interested whether data assimilation helps to bound the growth in uncertainty. In Figure 2, prior and posterior error variances are plotted as functions of depth for three selected times: $t = 10$, 40, and 70. Plots in rows (a) and (b) correspond to the case of $\alpha_m = 1/24$, and rows (c) and (d) to the case $\alpha_m = 0$. For rows (a) and (c) the model errors were not correlated in the vertical, while for rows (b) and (d) the errors in the model were vertically correlated with $\beta = 2$ in the covariance of (40). In all of these cases, the weight for the first baroclinic mode was the same.

In every computation, $E_{prior}(z)$ is symmetric with respect to $z = 0.5$, minimum at mid-depth, and maximum near the surface and bottom where the largest variations of the pressure are allowed by the model, based on our assumptions about the statistics of the errors in the equations. In case of Fig. 2a we see that the flow at the bottom is not recovered nearly as well as that at the surface ($E_{post}(z = 0)/E_{post}(z = 1) \approx 3.4$ at $t = 40$ and 70). If the errors in the governing equation are correlated in the vertical (see Fig. 2b), the ratio of the posterior variance at the bottom and the surface becomes smaller ($E_{post}(z = 0)/E_{post}(z = 1) \approx 1.9$ at $t = 40$ and 70). If there is no dissipation in the governing equation, data assimilation may to some degree restrict the growth of the error at the surface, but not at the bottom (see Fig. 2c). Correlation of the model errors in the vertical does not help to restrict the growth of the uncertainty at the bottom (see Fig. 2d). Thus, to have a model suitable for the study of the sequential algorithms, it is essential to have dissipation inside the domain, not only at the coast. Otherwise, the gain matrix will not become stationary.

4.2 Comparison of GIM and KF

For our coastal inverse model, the analytical representer solution can be used to compute the KF solution at any time t_k when measurements are available, by applying GIM in the time window $0 \leq t \leq t_k$ using only data available up to time t_k. This GIM solution at $t = t_k$ will be identical to what the KF would yield. By applying GIM repeatedly over larger and larger time intervals, involving more and more data, we can obtain the output of the KF as a function of time, and compare this with the solution of the GIM solution using data from the whole time interval $0 \leq t \leq T$.

It should be noted that in our coastal model the errors in the south boundary condition should be correlated in time (both physically, and for technical reasons; see KAME). At the same time the analysis of Section 2.2 is given for temporally uncorrelated model errors. The KF can be extended to allow for temporally correlated errors (Gelb 1974), although this would introduce some complications into the equations of Section 2.2. However, our computation of the KF solution, based on equivalence of GIM and KF at $t = T$, easily accommodates temporally correlated errors.

Prior and posterior variances are computed as functions of time at 6 points in the computational domain: one point each at the surface and the bottom at the north, middle and south cross-sections ($y = 0$, 1, and 2 correspondingly), all at an offshore distance $x = 0.2$. For these computations, weights are chosen so that the prior variance E_{prior} is on average close to 1 over the full assimilation time interval, and the decorrelation length scale is $L_y = 2$. The data weight $w_d = 100$ corresponds to $\sigma^2 = 0.01$.

We first consider the case when the error in the model solution is due to uncertainty in the wind forcing and initial/boundary conditions for the coastal trapped waves (Fig. 3a). In this case which we refer to as "c+IB" there are no errors in the governing equation or the IPV condition, so the representers have only a propagating component which moves from the south to the north, passing through the data locations at the time of measurement. At the south boundary, the GIM yields a posterior variance 1/3 that of the KF-derived solution. The advantage of GIM remains profound up to $t = 70$, when its error variance

starts increasing to match the performance of the sequential method at $t = T = 80$ as it must. It is quite clear why the GIM works better at the south boundary. Future data contain much information about the present flow south of all measurement points, and this information is not utilized by the KF. Past data provide maximum information somewhere to the north of the measurement points, and essentially no information at the south boundary. At the middle cross-section, the advantage of the GIM is still appreciable (about 20% of the variance), while at the northern boundary the future data are almost useless, and both KF and GIM perform with the same accuracy.

Next, consider the case "m+IPV" where we assume that the coastal boundary condition as well as the initial and boundary conditions for the traveling waves are perfect, and errors are due only to uncertainty in the governing equation and the IPV condition (Fig. 3b). In this case, the representer has a substantial stationary part and the advantage of the GIM can be subtle. In this example, data of relatively high quality totally control the solution at the time of the measurement, so that data obtained in the future or past bring very little new information. However, the advantage of GIM is greater if the data errors become larger (Fig. 3c, $w_d = 1$ instead of 100). Since we have assumed that the model errors are not correlated with depth, performance of both methods is relatively poor at the bottom, and the difference between GIM and KF is seen only at the surface.

Finally, we compute the variance as a function of x in the middle cross-section, at the surface and bottom, for time $t = 40$. The most distant data from the coast are at $x = 0.5$, and we would like to see how well the solution is restored farther offshore. In the case "c+IB" the data provide maximum correction to the solution at $x = 0$, and both the prior and posterior variances decay offshore exponentially (Fig. 4a). However, for the case "m+IPV", $w_d = 1$, the posterior variance increases beyond $x = 0.5$ (Fig. 4b). To diminish the effect of the error in the potential vorticity field at $x > 0.5$, measurements farther offshore would be necessary. In this case errors in the equations are not correlated in the vertical. At the surface, the posterior variance is reduced locally at the data locations indicating that the pressure field is undersampled for the assumed covariance structure.

If the errors in the governing equation and the IPV condition are correlated with depth ($\beta = 2$ in (40)), the performance at the bottom is much more like that at the surface. Then GIM is apparently better than KF at the bottom, not just at the surface, and the local depression of the posterior variance near the data sites that would be associated with smaller scales introduced by the higher modes is smoothed (Fig. 4c).

4.3 OI: the gain matrix and posterior variance

The results of Sect. 2.3 for OI were derived under the assumption that the model errors are uncorrelated in time. To apply these results to our coastal inverse model, we put $w_{IB} = \infty$, corresponding to zero variance in the south boundary condition, and move the boundary so far to the south that the exact boundary condition does not affect the solution in the region of interest ($0 \le y \le 2$). Due to dissipation, the prior covariance associated with the error in the open boundary condition decays alongshore as $e^{\alpha_c n \pi (y-L)}$, where n is the number of the baroclinic mode. Thus, for $\alpha_c = 1/24$, $L = 20$ is a safe choice for the south boundary. The extended computational domain is one of the prices we pay to use the simpler OI data assimilation routine.

For OI the forecast error covariance $\mathbf{C}_T$ must be chosen *a priori*. Recall that $\mathbf{C}_T$ can be interpreted as the covariance of the model solution error conditional upon the past data. In theory one should know the lagged prior covariances $\mathbf{S}_T$ (see (21)) to construct an optimal conditional covariance. A simpler approach was used by Oke et al. (2001) who essentially assumed that the spatial correlation structure of $\mathbf{C}_T$ is the same as that of the (unconditional) prior covariance $\mathbf{P}_{T,T}$. This avoids computation of lagged covariances, but is this assumption reasonable? For our simplified model we can explicitly compute the full covariances $\mathbf{C}_T\mathbf{H}'$ and $\mathbf{P}_{T,T}\mathbf{H}'$ and assess the validity and impact of this approximation. To compare the structure of the two covariances, we sample them on a uniform discrete grid: x is from 0.05 to 0.95 each 0.1, y is from 0 to 2 each 0.1, and z is from 0 to 1 each 0.1, a total of $M = 2,310$ mesh points.

The covariances $\mathbf{C}_T\mathbf{H}'$ and $\mathbf{P}_{T,T}\mathbf{H}'$ can be compared in several ways. First of all we

would like to find, for a range of covariance parameters, the scale factor $a \leq 1$, that makes $a\mathbf{P}_{T,T}\mathbf{H}'$ the closest to $\mathbf{C}_T\mathbf{H}'$. Specifically, we vary L_y and w_d, and find $a = a_{min}(L_y, w_d)$ that minimizes the norm

$$||\mathbf{X}(a)||_s = \text{the largest singular value of } \mathbf{X}(a), \tag{46}$$

where $\mathbf{X}(a) = \mathbf{C}_T\mathbf{H}' - a\mathbf{P}_{T,T}\mathbf{H}'$. Then, we plot the norm of the difference (46) computed for $a = a_{min}$ as a function of L_y and w_d (Fig. 5). The difference is apparent when w_d is large enough such that the use of the data makes sense. In the present example, if $w_d > 1$, the norm of the difference becomes larger with decreasing L_y. We take this result to indicate that accounting for lagged correlations in computing the gain matrix is probably more important if the model errors vary on shorter spatial scales. In a wind driven circulation model, the dynamical errors on the surface will probably have large decorrelation length scales associated with uncertainty of the wind stress. However, topography will introduce smaller scales. In our case, the difference is largest when $L_y = 0.5$, and it is smaller for $L_y = 0.2$. A possible explanation of this is that the covariance fields represented by the columns of both $\mathbf{C}_T\mathbf{H}'$ and $\mathbf{P}_{T,T}\mathbf{H}'$ become almost singular (δ-functions) when L_y is small, and the norm (46) is poor at distinguishing between such matrices.

We next look at the correlation structure of the two covariances. Each column of $\mathbf{C}_T\mathbf{H}'$ and $\mathbf{P}_{T,T}\mathbf{H}'$ represents a three-dimensional field giving the covariance between a particular observation location and all other points in the domain; for $\mathbf{P}_{T,T}\mathbf{H}'$ this is the representer. To illuminate differences in spatial structure, we normalize the covariances by their values at the corresponding observation location, and plot several alongshore sections (Fig. 6). If $L_y = 0.5$ (left panels in the Figure), the conditional covariance field is distorted in comparison with the unconditional (representer) field, with some decrease of the alongshore correlation scale. If $L_y = 2$ (right panels), the maximum of the conditional covariance is shifted to the south of the observation point (for an intermediate weight w_d, see plot (b)). With the larger data weight, when the present data alone provide good control of the solution and the past data bring almost nothing new, the maximum of the

covariance shifts back to the data location at the surface, but is still displaced at the bottom. Accordingly, at $L_y = 2$ the norm of (46) is small for large w_d (see Fig. 5).

Another way to compare $\mathbf{C}_T\mathbf{H}'$ and $\mathbf{P}_{T,T}\mathbf{H}'$ is to look at their singular vectors. By doing so we operate with all the columns of the matrices. In Fig. 7, we show alongshore sections of a few of the singular vectors of $\mathbf{P}_{T,T}\mathbf{H}'$ (on the left) and $\mathbf{C}_T\mathbf{H}'$ (on the right), $L_y = 0.5$. The dominant modes of $\mathbf{C}_T\mathbf{H}'$ that describe large scale alongshore variability are distorted and systematically shifted to the south.

To understand how much the structural difference between the conditional and unconditional prior covariances affects the solution, we compute the posterior variance of both the OI(C)- and OI(aP)-derived solutions at the same 6 points used in Sect. 4.2 (Fig. 8). As expected, the posterior variance curve for OI(C) merges with the curve for KF some time after the beginning of data assimilation, when the initial condition has been forgotten and the gain matrix for the KF has stabilized. The posterior variance for OI(aP) is larger than that for OI(C). If the approximate conditional covariance $a\mathbf{P}_{T,T}$ is used with optimal $a = a_{min}$, the difference is no more than 10% in our example (see Fig. 8 a, b). However, if a is misspecified, the difference will be larger. The limit $a \to 0$ corresponds to the case $\mathbf{G} \to 0$, and $E_{post} \to E_{prior}$. The limit $a \to 1$ (see Fig. 8 c, d) means that the effects of past data were disregarded during the construction of the gain matrix. As a consequence, the difference between posterior variance plots for KF and OI(aP) is larger in the area where the past data would have been significant, *i.e.* in the middle and at the north.

5 How bad is a wrong hypothesis about error covariances?

The analysis above is based on the assumption that the correct error covariances are used in the cost functional. However, the choice of the covariances is always a hypothesis. In addition, simplifications are typically made to ease computations. How much is the data

assimilation degraded if the error covariances are wrong? We can address this question using our simple model, by distinguishing between "true" and hypothesized covariances. The former are used to compute the prior variance, and the latter go into the cost functional and construction of representers or the gain matrix. For OI, expression (25) readily applies if $\mathbf{P}_{t,t}$, $\mathbf{S}_t$, $\mathbf{Q}_{t,t}$, and $\mathbf{R}_t$ are computed with the representers based on the true error covariances, while $\mathbf{K}$ is based on the hypothesized covariances. Similarly, for GIM (and thus also for KF), the expression for the posterior covariance that replaces (14) is

$$\overline{(\mathbf{U}-\tilde{\mathbf{U}})(\mathbf{U}-\tilde{\mathbf{U}})'} = \overline{\mathbf{U}\mathbf{U}'} - \mathbf{Q}\hat{\mathbf{P}}^{-1}\hat{\mathbf{Q}}' - \hat{\mathbf{Q}}\hat{\mathbf{P}}^{-1}\mathbf{Q}' + \hat{\mathbf{Q}}\hat{\mathbf{P}}^{-1}\mathbf{P}\hat{\mathbf{P}}^{-1}\hat{\mathbf{Q}}', \qquad (47)$$

where $\mathbf{P} = \mathbf{R} + \sigma^2\mathbf{I}_K$, and quantities without the hat, including the first term on the r.h.s. (prior covariance), are computed with the true error covariances, while those marked by the hat are computed with the hypothesized covariances.

A number of statistical parameters such as weights and decorrelation length scales need to be prescribed to define the covariances. As we have apparatus for the assessment of the effect of their misspecification, a large number of computations could be produced. We choose two examples illustrating the effect of misspecification of the correlation structure. In each example, we compare the performance of the methods at time $t = 70$, after the initial condition has already been forgotten, but when there are still future data containing potentially valuable information. Plots show the variance as a function of depth. The posterior variance is computed with both right and wrong hypotheses about the input error covariances. Results for OI are obtained using the conditional covariance $\mathbf{C}_T$ in the gain matrix. At time $t = 70$, the variance for OI(C) coincides with that for KF. The south boundary is again at $L = 20$, far from the region of interest.

Example 1: The uncertainty in the model solution is due to the error in the governing equation (31) while the coastal boundary condition (32) is exact. For true error statistics the model errors $\epsilon^{(m)}$ are correlated with depth ($\beta = 2$), while the assumed hypothesis is that the errors are not correlated ($\beta = 0$), or vice versa (Fig. 9). First, if in fact $\beta = 2$ (Fig. 9a), GIM with the misspecified error covariance ($\beta = 0$) is significantly less

efficient than the GIM with the correct covariance, both at the surface and the bottom. In contrast, when $\beta = 0$ (Fig. 9b), misspecification has little effect on the performance. In this example, we are safe if we assume errors are correlated whether they are or not. With the coastal boundary condition exact the representers are dominated by the stationary part, and the GIM has little advantage over the sequential algorithms. Thus, analysis for OI gives posterior variances close to those achieved by GIM (Figs. 9c, and d). In case the errors are indeed correlated in the vertical, specification of the right covariance is more important than the use of future data (compare the dashed line, plot (a), and the solid line, plot (c)).

Example 2. Let us turn to the case where GIM has a significant advantage over the sequential schemes. That is, let the error in the model solution be due to uncertainty in the wind forcing while the equation for the variation of the potential vorticity (31) is exact; consider the variance at $y = 2$, *i.e.* south of all the data. The true alongshore error decorrelation length scale is $L_y = 0.5$, and the misspecified value is $L_y = 2$, or vice versa (Fig. 10). Overestimating the decorrelation length scale when it is small (Fig. 10a) is apparently more dangerous than underestimating the decorrelation length scale when it is large (Fig. 10b). Refer to Table 1 where we show the ratio of the posterior variances computed with wrong and right input statistics: the larger the value in the table, the more sensitive the data assimilation is to the choice of the prior error hypothesis. Use of the correct decorrelation length scale L_y is more important for GIM than OI. However, GIM yields a smaller variance than OI.

In reality, the general situation is that wind forcing varies on large scales compared to the size of our domain. In this case GIM with the misspecified error decorrelation length scale yields the same performance as OI with the right prior error covariance (compare the dashed line, plot (b), and the solid line, plot (d)).

It may be noticed that assuming the errors have too large a scale in the vertical does not cause problems (example 1, see Fig. 9b), but overspecification of the horizontal scale does indeed cause problems (example 2, see Fig. 10a). Equation (31) provides sufficient

smoothing in the vertical to the singularities in the representer solution, so that the first mode is dominant in this solution even if the covariance (40) is singular ($\beta = 0$), as in example 1. In this case, modal amplitudes of the representer decrease as n^{-2}, where n is the mode number (see KAME). Excessive smoothing in the vertical means dampening higher, relatively insignificant modes, which is harmless. In contrast, in the alongshore direction, the dynamics does not provide an intrinsic dominant length scale. The alongshore length scale is determined by the scale of the wind forcing error, which for our model translates into the error in the coastal boundary condition (32), as discussed in example 2. Now excessive smoothing in the alongshore direction prevents the model from interpreting small scale variations presented in data as signal, so the data assimilation performance is degraded.

6 Summary

We have compared performance of different data assimilation schemes with a simplified coastal baroclinic model. The analytical representer solution allows us to compute the posterior error variance of the GIM, KF and OI solutions. For KF and OI, we do not need to integrate the equations explicitly from one assimilation cycle to another, but rather can use results obtained in the framework of GIM. The tools of statistical analysis derived here can also be applied to assess the impact of misspecified input error covariances. These tools are independent of a particular dynamical model, and can be used with other applications.

Although our model is highly idealized, it sheds light on a number of issues that would be relevant in a more realistic environment. In comparison with the previous study of Scott et al. (2000), retaining alongshore and temporal variability allowed us to analyze the use of distant data. GIM has an advantage over the sequential algorithms since it uses all the data, including future data, in an optimal way to obtain an estimate of the flow. In a practically relevant case, GIM with misspecified input error statistics produces

a result of the same quality as the sequential methods with correctly specified input error covariances.

In the present study, the variational method had the greatest advantage over sequential schemes when the coastal boundary condition was assumed imperfect, while the governing equation describing evolution of the potential vorticity was a strong constraint. However, we do not want the reader to get the impression that GIM generally works better in the strong constraint case than in the weak constraint case. Cases where either the coastal boundary condition or the governing equation are imperfect have been separated in an attempt to systematize the analysis. In the former case, the representer has only a propagating component, while in the latter case a substantial stationary component is present (KAME). In our dynamical model the wind stress forces the coastal boundary condition that describes the balance of the surface Ekman and interior cross-shore flows. In realistic coastal circulation models, the wind stress is probably a significant source of error in model solutions (see Oke et al. 2001). We have tried to emphasize the role of data assimilation in reducing this error, rather than to derive any conclusions about the relative value of strong and weak constraint model formulations. Even in the case where the governing equation is a weak constraint, the advantage of GIM over KF is significant if the data error becomes large.

To provide a concise description, we confined our study to a particular observation system which would be relevant to the present HF radar system currently in operation at the mid-Oregon coast. Based on our results, we may presume that deployment of more radars to the north or south of our test region (which was about 50 km alongshore) would help to improve prediction in the test region. Since information propagates with the long coastal trapped waves from south to north, the new data would help to eliminate the error associated with misspecified wind stress or boundary conditions at the southern edge of the domain. However, data obtained far up or down the coast (farther than $\sim$400 km) would probably not contribute much because of dissipation. Information about 2nd and higher baroclinic modes becomes insignificant on even shorter length scales.

Analysis of the OI sequential scheme shows how lagged covariances of the model solution error can be used to optimize the form of the gain matrix (see (18) and (21)). Even with a complex primitive equation model $\mathbf{P}_{T,T}\mathbf{H}'$ can be estimated based on the ensemble of the model runs (*e.g.*, Oke et al. 2001). The elements $\mathbf{Q}_{T,T-t} = \mathbf{P}_{T,T-t}\mathbf{H}'$, necessary to build $\mathbf{S}_T$ in (21), can be estimated in a similar way from the same ensemble. In practice, a restricted number of $\mathbf{Q}_{T,T-t}$ need be computed since lagged covariances corresponding to large differences $T-t$, *e.g.*, more than 3 days in our example, are negligible because of dissipation. Note that in (26) the scaling factor a for the approximate forecast error covariance gets mixed up with the data variance σ^2 which complicates specification of this statistical parameter. Computation of the optimized gain matrix would make specification of a unnecessary.

In our computational example, the difference in the performance of OI(aP) was nearly as good as OI(C) or KF. However, we have observed that the difference in structure between the conditioned and unconditioned prior covariances, important for OI, can be relatively large when the error decorrelation length scale is small. Such short scales may be introduced by the variable bathymetry and curved coastline. Topography will also influence the way propagating waves carry information. These topics will be subjects of future study.

Acknowledgments. The research was supported by the Office of Naval Research (ONR) Ocean Modeling and Prediction Program under Grant N00014-98-1-0043.

References:

Bennett, A. F., 1992: *Inverse methods in physical oceanography.* Cambridge University Press, 346 pp.

Cohn, S. E., 1997: An introduction to estimation theory. *J. of the Meteorological Society of Japan*, **75**, No. 1B, 257-288.

Daley, R., 1991: *Atmospheric data analysis.* Cambridge University Press, 457 pp.

Gelb, A. (ed.), 1974: *Applied Optimal Estimation.* MIT Press, Cambridge, Mass., 374 pp.

Gelfand, I. M., and Fomin, S.V., 1963: *Calculus of variations.* Prentice Hall, Englewood Cliffs.

Kosro, P. M., Barth, J. A., & Strub, P. T., 1997: The coastal jet: observations of surface currents over the Oregon continental shelf from HF radar. *Oceanography*, **10**, 53-56.

Kurapov, A. L., Allen, J. S., Miller, R. N., & Egbert, G. D., 2001: Data assimilation in a baroclinic coastal ocean model: generalized inverse, *J. Geophys. Res. - Oceans*, submit.

Miller, R.N., 1996: Introduction to the Kalman filter. *Proc. ECMWF Seminar on Data Assimilation, ECMWF*, Shinfield Park, Reading, UK, 2-6 September, 1996, 47-59.

Oke, P. R., Allen, J. S., Miller, R. N., Egbert, G. D., & Kosro, P. M., 2001: Assimilation of surface velocity data into a primitive equation coastal ocean model (submitted to *J. Geophys. Res.*).

Scott, R. K., J. S. Allen, G. D. Egbert, and R. N. Miller, 2000: Assimilation of surface current measurements in a coastal ocean model. *J. Phys. Oceanogr.*, **30**, 2359-2378.

Talagrand, O., 1997: Assimilation of Observations, an Introduction. *J. of the Meteorological Society of Japan*, **75**, No. 1B, 191-209.

Table 1. **Ratio of posterior variances computed with wrong or right error decorrelation length scale for wind forcing. Values of L_y in parentheses next to E_{post} show the hypothesis scale.**

	"truth": $L_y = 0.5$ $E_{post}(L_y = 2)/E_{post}(L_y = 0.5)$	"truth": $L_y = 2$ $E_{post}(L_y = 0.5)/E_{post}(L_y = 2)$
	GIM	
surface	2.4177	1.6658
bottom	1.8614	1.2877
	OI	
surface	1.8615	1.7241
bottom	1.4965	1.3128

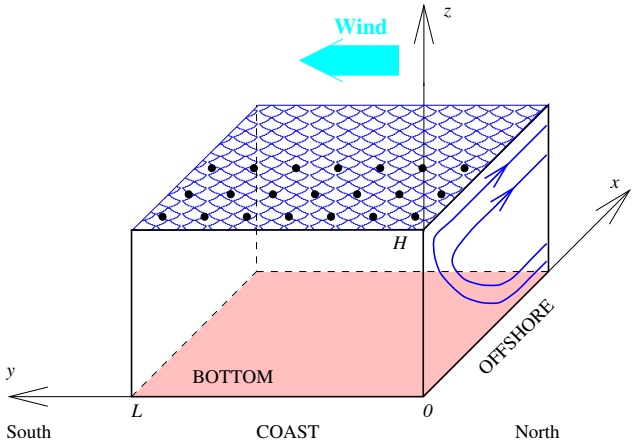

Figure 1. Model setup. Bullets at the surface show locations of the observations used in the computations.

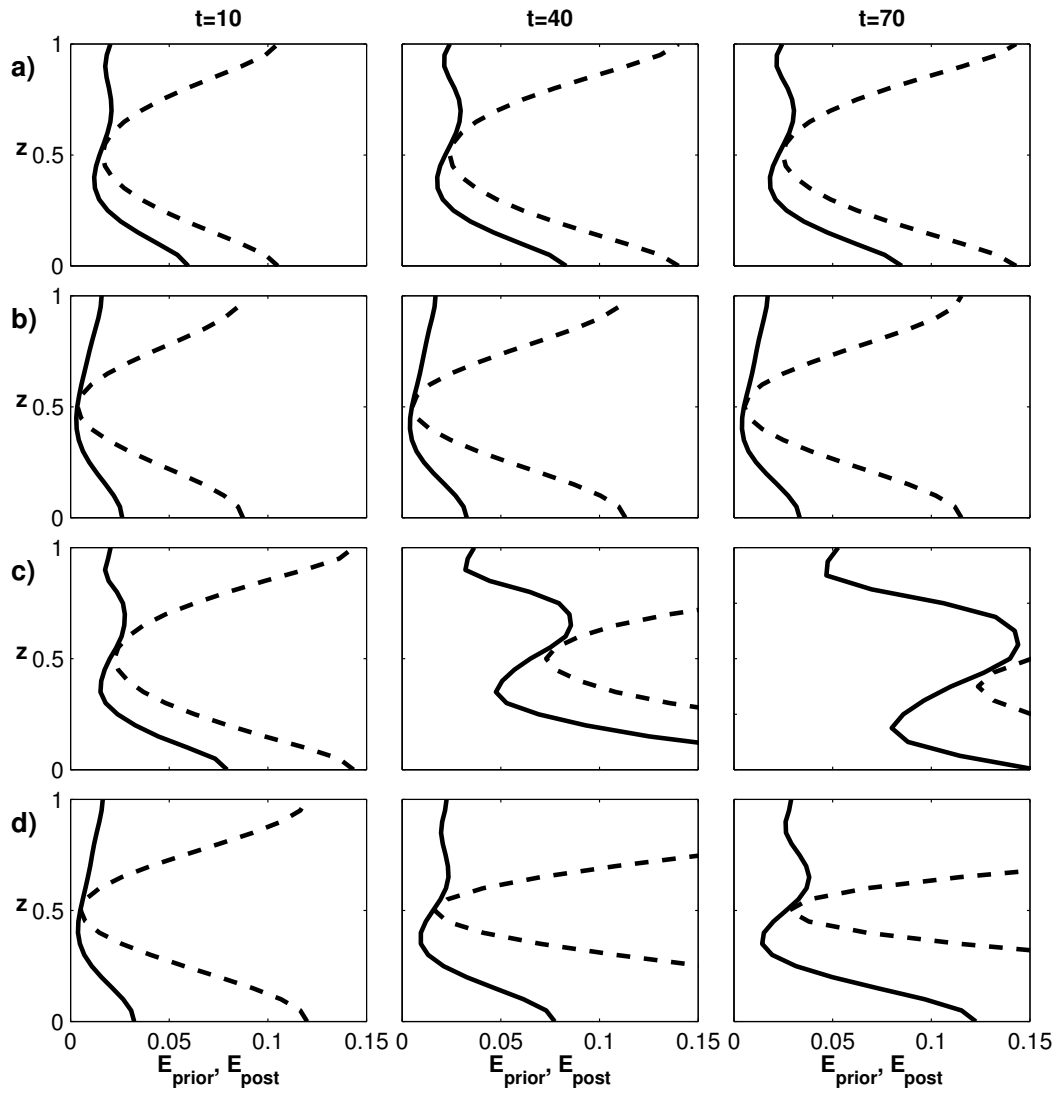

Fig. 2. Prior (dashed lines) and posterior (solid lines) variance as a function of z, at $x = 0.2$, $y = 1$; $w_m = 1/\pi^\beta$, $w_d = 5$, and the other weights are ∞. Each column corresponds to a specific time (10, 40, or 70). Rows: (a) $\alpha_m = 1/24$, $\beta = 0$; (b) $\alpha_m = 1/24$, $\beta = 2$; (c) $\alpha_m = 0$, $\beta = 0$; (d) $\alpha_m = 0$, $\beta = 2$.

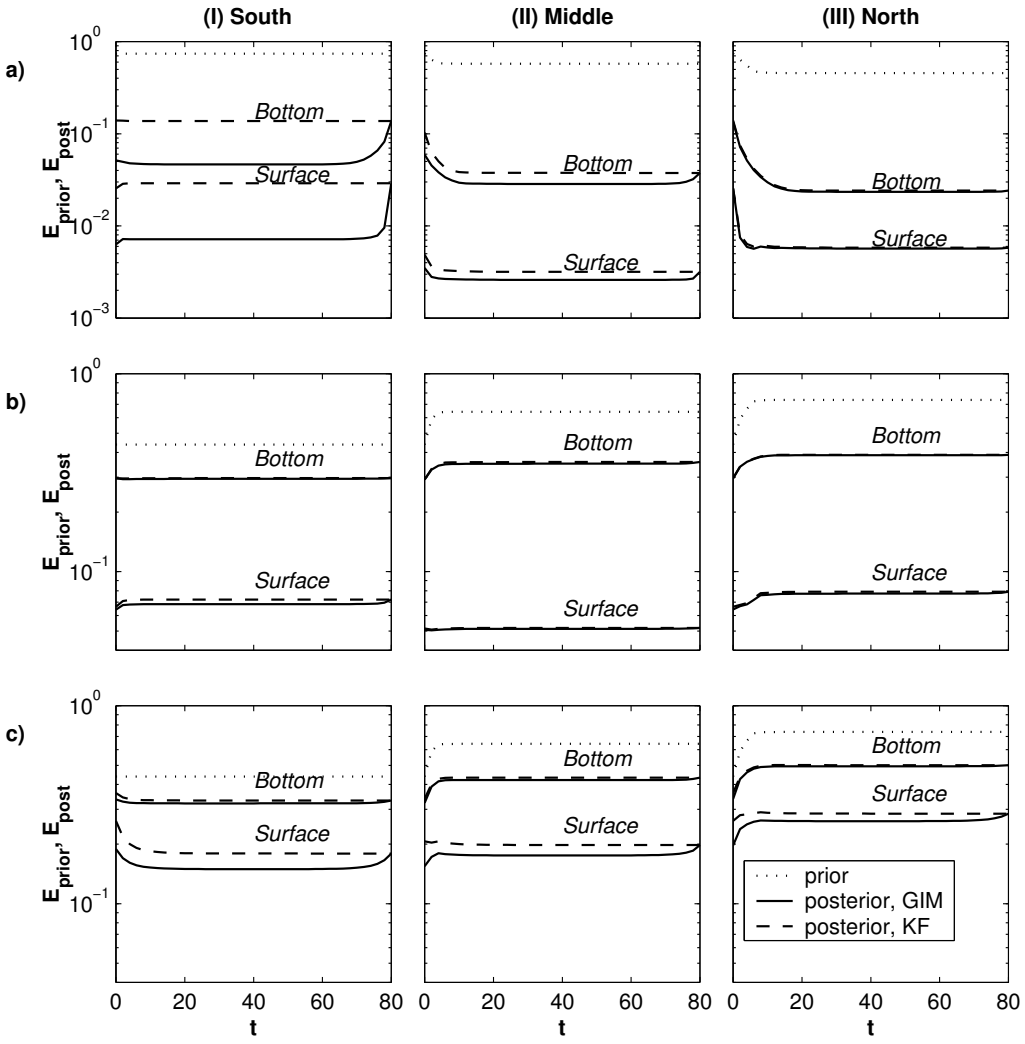

Fig. 3. Prior and posterior variance of the GIM- and KF-derived solutions vs. time at 6 different points, all at the off-shore distance $x = 0.2$. Columns: (I) South ($y = L = 2$), (II) Middle ($y = 1$), and (III) North ($y = 0$). Weights: line (a) $w_m = w_{IPV} = \infty$, $w_c = 10$, $w_{IB} = 0.084$, $w_d = 100$; (b) $w_m = 0.2$, $w_{IPV} = 0.017$, $w_c = w_{IB} = \infty$, $w_d = 100$, $\beta = 0$; (c) the same as (b), but with the lower data weight $w_d = 1$.

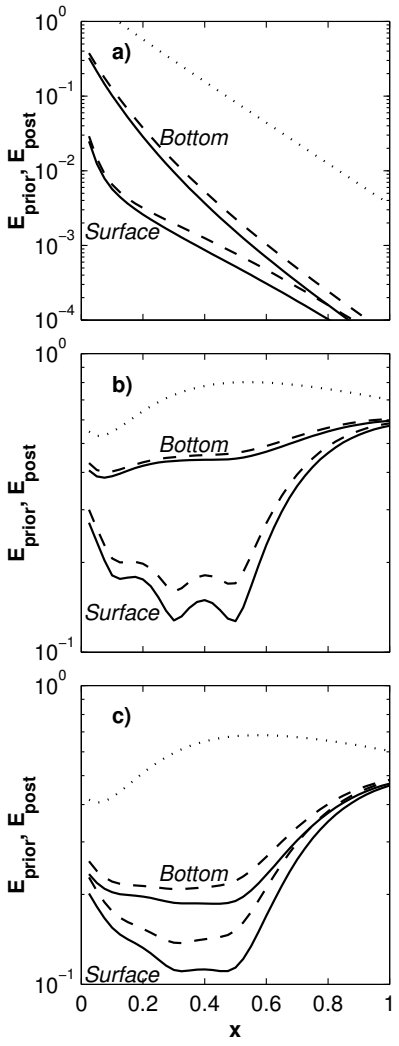

Fig. 4. Variance of the GIM- and KF-derived solutions *vs.* x at the surface and bottom, $y = 1$, $t = 40$, surface and bottom. Legend – see Fig. 3. (a) case "c+IB", $w_m = w_{IPV} = \infty$, $w_c = 10$, $w_{IB} = 0.084$, $w_d = 100$; (b) case "m+IPV", $\beta = 0$, $w_m = 0.2$, $w_{IPV} = 0.017$, $w_c = w_{IB} = \infty$, $w_d = 1$; (c) case "m+IPV", $\beta = 2$: $w_m = 0.2/\pi^\beta$, $w_{IPV} = 0.017/\pi^\beta$, $w_c = w_{IB} = \infty$, $w_d = 1$.

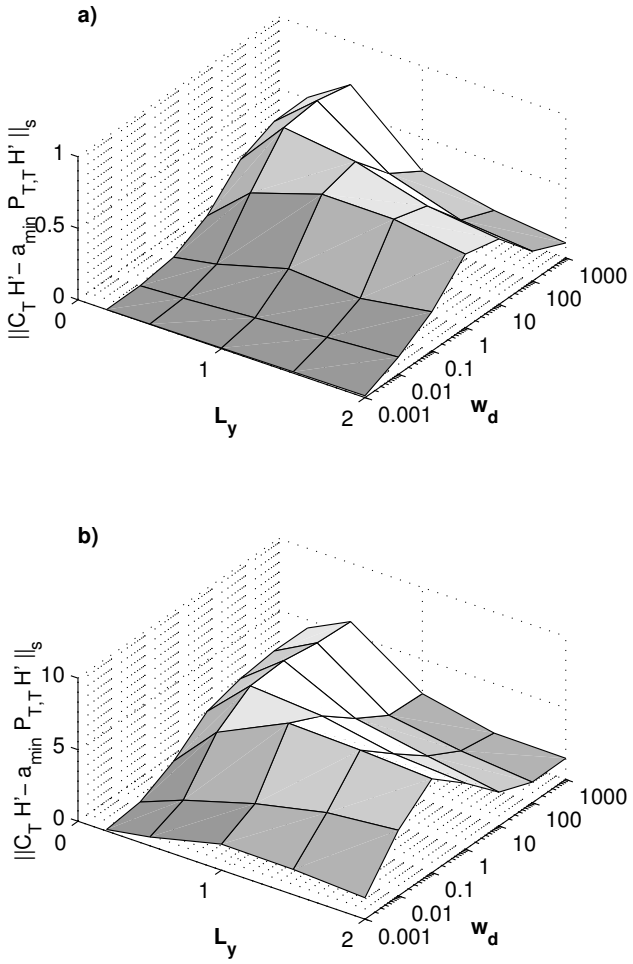

Fig. 5. Norm (46) of $\mathbf{C}_T\mathbf{H}' - a_{min}\mathbf{P}_{T,T}\mathbf{H}'$ as a function of L_y and w_d: a) $w_m = \infty$, $w_c = 10$; (b) $w_m = 0.2$, $w_c = \infty$.

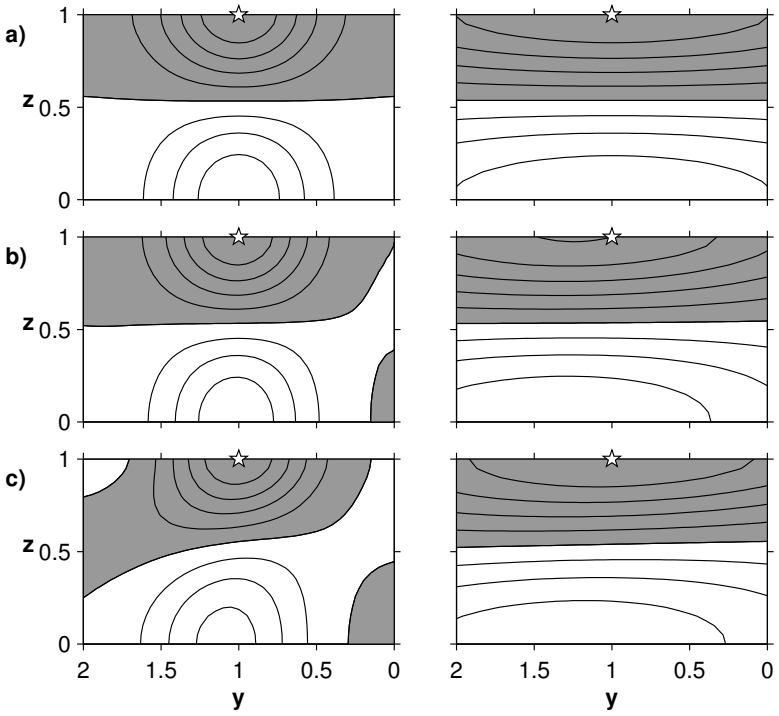

Fig. 6. Covariance fields corresponding to a column of $\mathbf{P}_{T,T}\mathbf{H}'$ and $\mathbf{C}_T\mathbf{H}'$ normalized by the value at the datum site $(x_k, y_k) = (1, 0.1)$ (denoted by star), shown in the alongshore section $x = 0.1$; $w_m = 0.2$, $w_c = \infty$, $\beta = 0$. Left plots: $L_y = 0.5$, right plots: $L_y = 2$. Shaded area is for the positive values, contour offset is 0.2: (a) $\mathbf{P}_{T,T}\mathbf{H}'$; (b) $\mathbf{C}_T\mathbf{H}'$, $w_d = 10^{-1}$; (c) $\mathbf{C}_T\mathbf{H}'$, $w_d = 10^3$.

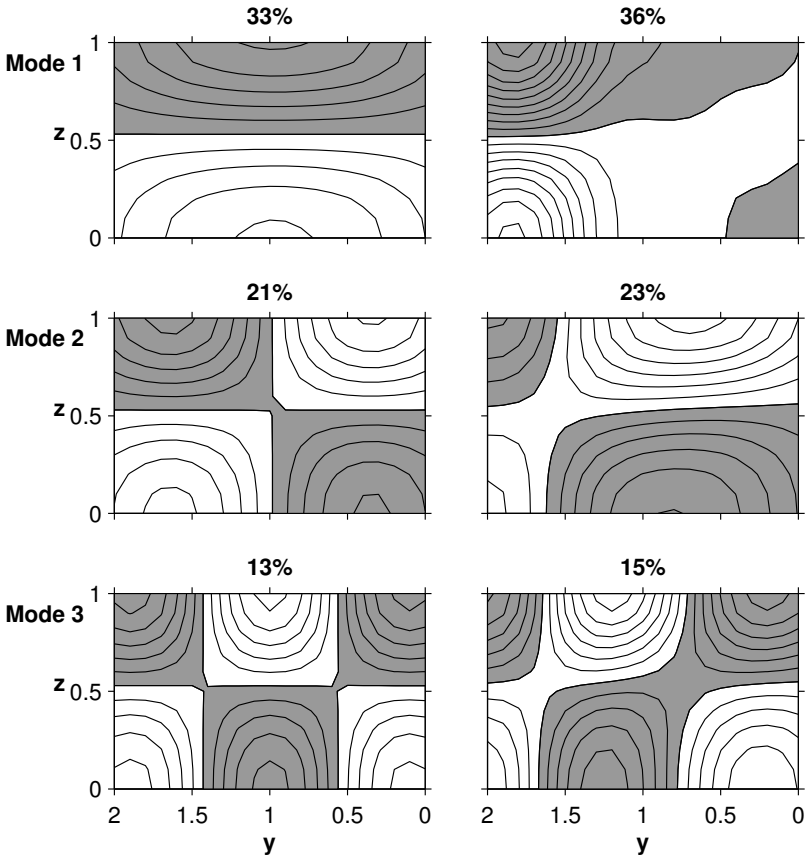

Fig. 7. First singular vectors of $\mathbf{P}_{T,T}\mathbf{H}'$ (left panels) and $\mathbf{C}_T\mathbf{H}'$ (right panels) shown in the alongshore section $x = 0.15$; shaded area is for the positive values, contour offset is 0.01. $L_y = 0.5$, $w_m = 0.2$, $w_c = \infty$, $w_d = 100$. Percent numbers indicate how much variability is explained by the mode.

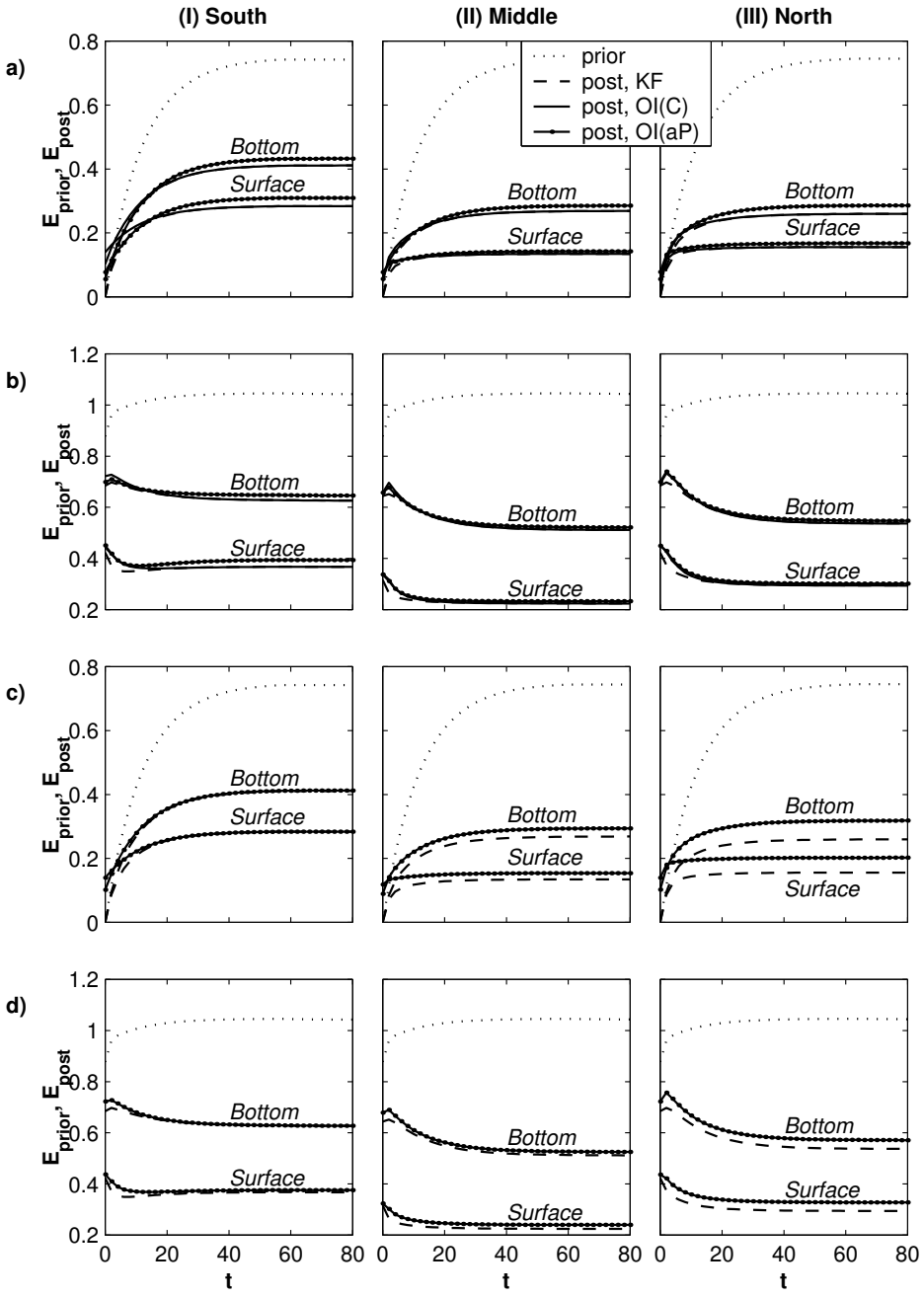

Fig. 8. Variance of OI- and KF- derived solutions vs. time at 6 different points at $x = 0.2$, $L_y = 0.5$. Columns: (I) South ($y = L = 2$), (II) Middle ($y = 1$), and (III) North ($y = 0$). Rows: (a) $w_m = w_{IPV} = \infty$, $w_c = 1$, $w_d = 1$, $a = a_{min} = 0.5$; (b) $w_m = 0.2$, $w_{IPV} = 0.017$, $w_c = \infty$, $w_d = 1$, $a = a_{min} = 0.45$; (c) and (d) are the same as (a) and (b), correspondingly, but with $a = 1$.

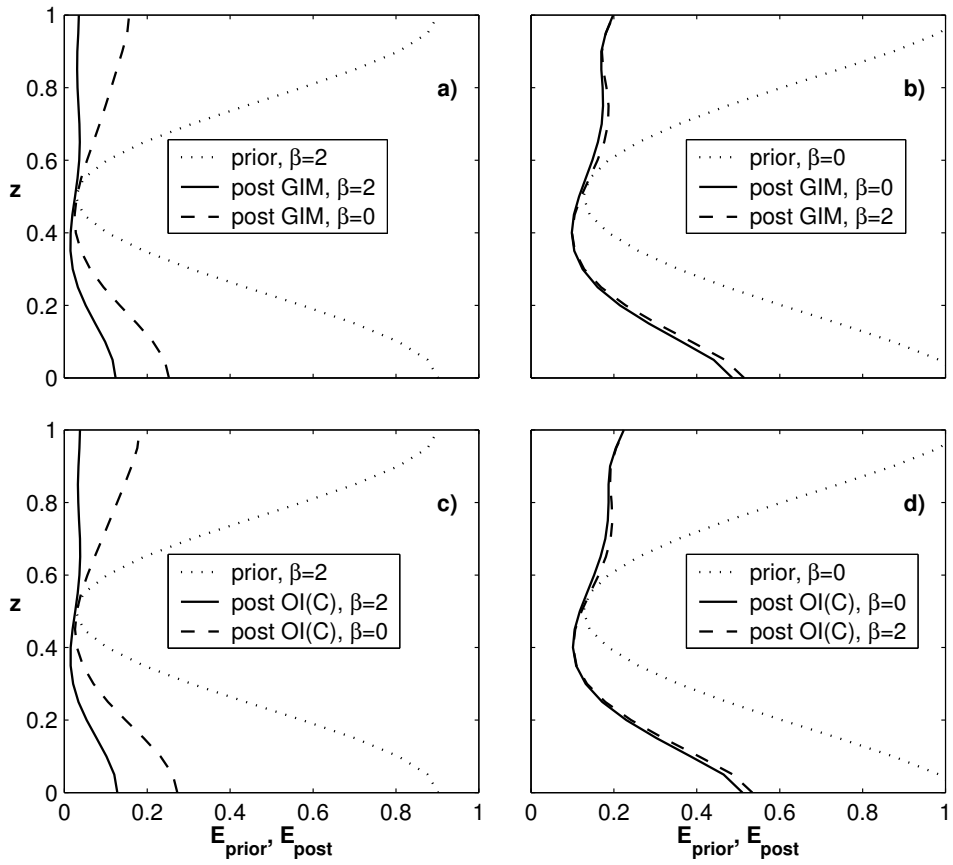

Fig. 9. Effect of misspecification of the model error covariance in the vertical: prior and posterior variance are shown as functions of z at $x = 0.2$, $y = 1$, $t = 70$. $w_m = 0.2/\pi^\beta$, $w_c = \infty$, $w_d = 1$, $L_y = 0.5$. A legend for each plot shows the value of the smoothing parameter β: the number next to curve "prior" is the "true" statistical parameter for all the curves on the plot; the numbers next to curves "post" (posterior variance) are our statistical hypothesis, right or wrong. Cases (a), (b) are for the GIM; (c), (d) are for the OI.

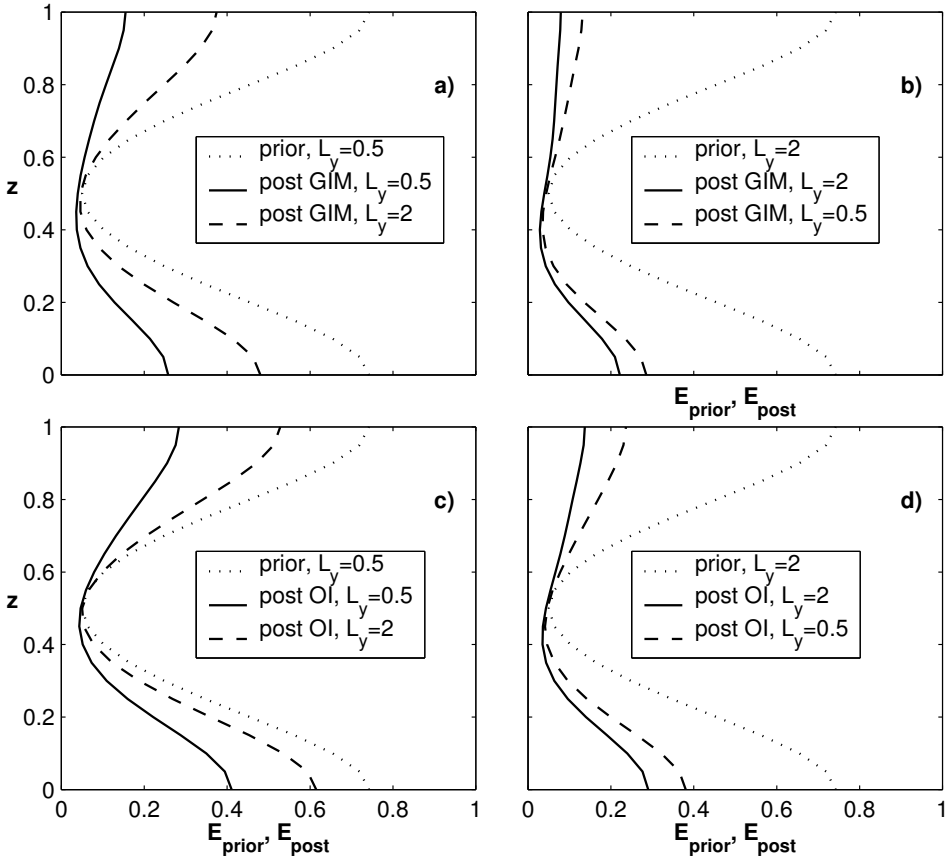

Fig. 10. Effect of over- or underestimation of the error decorrelation length scale for the wind stress: prior and posterior variance are shown as functions of z at $x = 0.2$, $y = 2$, $t = 70$. $w_m = \infty$, $w_c = 1$, $w_d = 1$. A legend for each plot shows the value of the smoothing parameter L_y: the number next to curve "prior" is the "true" statistical parameter for all the curves on the plot; the numbers next to curves "post" (posterior variance) are our statistical hypothesis, right or wrong.Cases (a), (b) are for the GIM; (c), (d) are for the OI.